PCCP

RSC Publishing

PAPER

Anchoring sites to the STM tip can explain multiple peaks in single molecule conductance histograms

Cite this: *Phys. Chem. Chem. Phys.*, 2013, **15**, 1526

S. Alexis Paz, Martin E. Zoloff Michoff, Christian F. A. Negre, Jimena A. Olmos-Asar, Marcelo M. Mariscal, Cristián G. Sánchez and Ezequiel P. M. Leiva*

Received 29th October 2012,
Accepted 20th November 2012

DOI: 10.1039/c2cp43811a

www.rsc.org/pccp

Accelerated molecular dynamics and quantum conductance calculations are employed to shed light onto the electrochemical properties of the Au|1,8-octanedithiol|Au junction. Widely different contact geometries with varying degrees of roughness are examined. Strikingly, the two extreme situations considered in this work, tip–tip and tip–perfect surface junctions, give almost indistinguishable conductances. This result contrasts the usual notion that different S–Au bonding geometries combined with molecular torsions provide the explanation for the experimentally observed sets (low, medium, high) of conductance peaks. In this work, we provide an alternative explanation for the occurrence of these sets in terms of the specific anchoring sites of the molecule to the tip, which in turn determines the interaction of a portion of the carbon chain with the tip.

1 Introduction

The potential use of single molecules as components of electronic devices has promoted a profusion of experimental[1–10] and theoretical[11–17] work. Besides the obvious advantages in miniaturization of such devices, the chemical versatility of molecules allows the exploration of new device design methods based on controlling the function through chemical tailoring.[18–20] However, for these desirable goals to be experimentally accessible it is mandatory to solve several problems such as reliably controlling the coupling to contacts,[17,21] reducing electron–phonon interactions in order to improve stability,[7] and design reliable and efficient gating mechanisms that can control current flow through the molecule in order to obtain devices that can function as a transistor,[22] just to mention a few.

Concerning the understanding of electronic transport properties of resistor like devices, the most simple and surprisingly challenging system appears to be the one formed by an alkanedithiol molecule trapped between two Au nanotips. The electromechanical behavior of this system has also shown to be difficult to understand, and the wide range of disparate results reported in the literature makes this understanding even harder.[23] Depending on the experimental method employed, repeated conductance measurements show histograms with more than one peak. This is the case of the measurements described in ref. 1, 4 and 24, where three fundamental conductance peaks were found. Haiss *et al.*[24] have attributed the three fundamental conductance contributions to different molecule–electrode contact geometries, namely a loose contact with the tip and the surface, thiol adsorption at step edges, and attachment of both sulfur head-groups to step edges respectively. While the first type of contact should be favored in the case of the so-called I(t) type of experiments,[6] where one of the ends of the molecule is picked by a STM tip held at a constant distance from the surface, the other two could arise when a close interaction of the tip with the surface is allowed, or when the surface shows a preexisting important number of defects.

In a previous work we have used an accelerated dynamics scheme to sample the configuration space of the molecular structure attached to two metallic electrodes in order to study the dependence of conductance on the distance between the metallic contacts and the influence of the internal molecular conformation.[25] In the present work we extend this methodology to study the influence of different structures of the metal contacts on the conductance.

2 Methodology

2.1 Hyperdynamics

To perform the configurational sampling of the system, the hyperdynamics (HD) method, as developed by Voter,[26] was applied using an in-house developed code. This method allows an enhanced sampling of molecular configurations (with barriers of up to 0.25 eV, see ref. 27) to be employed as a basis

INFIQC – Departamento de Matemática y Física, Facultad de Ciencias Químicas, Universidad Nacional de Córdoba, Córdoba, Argentina.
E-mail: eleiva@fcq.unc.edu.ar

for conductance calculations. We will briefly explain the hyperdynamics method, by summarizing the main concepts below. This method accelerates the exploration of a system undergoing rare events, without losing the main features of its natural dynamics. The key is to transform the potential energy surface (PES) of the system $V(r)$ with the addition of a bias function ΔV_b, as shown in eqn (1).

$$V_b(r) = V(r) + \Delta V_b(r) \quad (1)$$

This transformation reduces the energy barriers of the system, making the escape from trapping minima faster and allows an efficient sampling of the configuration space in a reasonable simulation time. However, to recover the average of any property, such as molecular conductance, the sampled configuration must be re-weighted using a ''boost'' factor that depends on the extent of the applied bias (refer to eqn (2)).

$$\langle A \rangle_V = \langle A w(r) \rangle_{V_b} \quad \text{where} \quad w(r) = \frac{e^{\beta \Delta V_b(r)}}{\langle e^{\beta \Delta V_b(r)} \rangle_{V_b}} \quad (2)$$

According to Voter,[26] real time can also be recovered through this re-weighting, but an extra restriction must be added: the bias must vanish at transition states. However, this restriction is not required for the calculation of thermodynamic properties, as it is the case of conductance. Therefore, for any bias function that allows a good sampling of the PES (*i.e.* maintaining the underlying shape) the re-weighting equations are usable.

In our previous work we used the bias function proposed by Hamelberg *et al.* applied to dihedral angles of the octanedithiol molecule.[28] However, in the present work we use an even simpler scheme: we apply to dihedrals the bias function given by eqn (3).

$$\Delta V_b(r) = (\alpha - 1)V(r) \quad (3)$$

Here the α parameter acts as a ''compression factor'' of the PES, by making the energy landscape shallower, while keeping the positions of local extrema unchanged. The use of this factor has the consequence of improving sampling, since all energy barriers are scaled by this factor. This compression scheme has been successfully used by Becker and Fichthorn[29] to study desorption of *n*-alkanes from the basal plane of graphite. Our choice is based on the fact that, for enhanced sampling purposes, we do not need to set the condition that the bias must vanish at the transition states. Since there are no transitions between the original PES and the biased one during the simulation, the derivative of the latter remains continuous. The α factor used here is 0.5.

2.2 Model and simulation set up

To emulate the metal–molecule–metal junctions obtained with the different experimental methods, we employ an atomistic model representing an octanedithiol molecule trapped in between a gold tip-like structure and a gold substrate with different roughnesses. Concerning the interatomic potentials, the same semiempirical description as that of our previous work[25] was used. The molecule–metal interaction was modeled with the semiempirical potential of Olmos-Asar *et al.*,[30] based on density functional theory (DFT) calculations and a bond-order Morse-like potential. It is noteworthy that this potential was developed to simulate the Au–S interaction in different S and Au coordination environments. The latter is suitable for simulating the different gold–molecule–gold junction systems presented in this work. Intra-molecular interactions within the octanedithiol molecule were represented using the all-atom optimized potentials for liquid simulations (OPLS-AA) force field. The parameters were extracted from ref. 27. In the case of the metal–metal interactions, we used the Second-Moment Approximation of Tight Binding (SMTB), which takes into account the many-body character of the metallic bond and has been found to reproduce most of the characteristic properties of gold. The parameters of this potential were taken from ref. 31.

In order to explore plausible scenarios representing different conditions of the substrate, we used four different types of tip–substrate metal junctions for our simulations. The tips of all junctions were built by stretching a 400 atoms gold cube with fcc structure from two of its opposite faces until rupture at a rate of 2 Å ps^{-1}. To model substrates with a high degree of roughness, such as those probably formed with the STM break-junction method, we used a second tip instead of a ''traditional'' perfect slab (see Fig. 1a). This yields a configuration referred to as tip–tip (T–T) junction. For modeling substrate

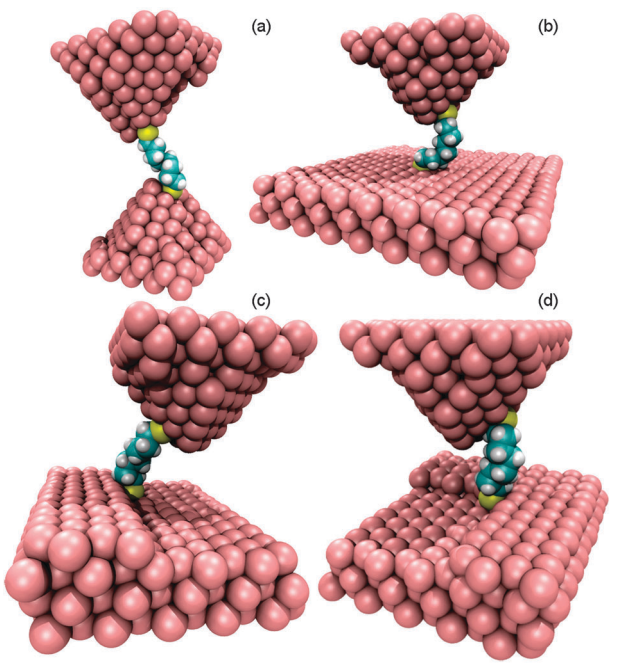

Fig. 1 Scheme of the atomistic models employed in the present simulations to represent surfaces with different roughnesses: (a) tip–tip (T–T) junction, (b) tip–perfect surface (T–P) junction, (c) tip–step (T–S) junction, (d) tip–kink (T–K) junction. Au atoms are shown in pink, S atoms in yellow, C atoms in blue and H atoms in white. The upper and bottom layers of Au atoms were kept fixed during the dynamical simulations. The figures are snapshots taken from the corresponding simulations. All atoms in the system were included in the conductance calculations.

surfaces with a low degree of roughness, such as those probably involved in the I(t) technique, we used a pristine (111) fcc surface as a substrate. This configuration is referred to as tip–perfect surface (T–P) junction (see Fig. 1b). Two additional systems of intermediate roughness were considered by adding defects to the perfect (111) surface, namely, a step, referred as tip–step (T–S) junction (see Fig. 1c) and a kink, referred as tip–kink (T–K) junction (see Fig. 1d).

To compare the behavior of these different systems, simulations were performed maintaining a gap distance of (10 ± 0.2) Å between the two metal contacts. For all the simulations the top and bottom gold layers of the upper/lower tips/substrate, respectively, were fixed at their bulk lattice positions. The metal contacts and the molecule were assembled together and were allowed to relax during 1 ns at constant temperature (300 K) using the Ermak algorithm[32] with a friction coefficient of 1 ps^{-1}. The latter was the sampling algorithm adopted for all the simulations presented in this work. All junction systems were equilibrated at this temperature during 10^6 HD steps.

At the end of Section 3 we consider another metal–molecule–metal junction constructed by adding to the perfect (111) surface an island which contains defects as those shown previously. The conductance in this system was measured at different tip–surface gap distances.

2.3 Conductance

The current flowing through the molecule coupled to two electron reservoirs (leads) was calculated by applying the Landauer–Büttiker formula.[33,34] The electronic structure is represented through the Extended Hückel Hamiltonian. Although conductance values may change if a higher level of theory is employed,[38] relative trends are expected to remain the same. This is because the conductance of the system is essentially determined by the atomic connectivity and bond lengths, which are outcomes of the molecular dynamics simulation. The transmission function was obtained from the Fisher–Lee equation[35] as follows:

$$G = \frac{2e^2}{h}\mathrm{Tr}(G_{\mathrm{dev}}{}^{+}(z)\Gamma_{\mathrm{L}}(E_{\mathrm{F}})G_{\mathrm{dev}}{}^{-}(z)\Gamma_{\mathrm{R}}(E_{\mathrm{F}})) \qquad (4)$$

where $G_{\mathrm{dev}}{}^{-/+}$ is the retarded and advanced green function matrix for the system. The presence of the leads was modeled by shifting the onsite atomic orbital energy for those orbitals that are in direct contact with the leads. This shifting is an energy imaginary value that enters in the Hamiltonian *via* the coupling matrices $\Gamma_{\mathrm{L/R}}(E)$ for the left and right leads. This imaginary energy value was fitted to recover the quantum value for conductance $G_0 = 2e^2/h$ for a perfect gold atom chain. The same imaginary value was used for the rest of the calculations. The details of the shifting procedure are explained in ref. 25 and the resulting conductance values calculated within this method are in good agreement with experimental data. All conductance histograms presented in this work are constructed with 1000 frames taken from the corresponding HD simulations, considering all atoms of the system.

3 Results and discussion

In ref. 4, the low conductance set of histograms was attributed to the occurrence of gauche defects in the alkane chain. For this reason, one hypothesis to be analyzed is whether molecular twisting is responsible for the occurrence of multiple conductance values. To analyze the configurational twist of the molecule, two parameters were defined, evaluated and analyzed: the S–S distance in the molecule $d_{\mathrm{S–S}}$ and the dihedral signature (Θ_{S}). The latter is defined as $\Theta_{\mathrm{S}} = \frac{1}{\pi}\sum_{i=1}^{n}|\theta_i|$ where θ_i is the ith dihedral angle of the molecule. In the case of the octanedithiol molecule, the sum is taken over the seven main dihedral angles (five of these angles are calculated considering four consecutive C atom groups and two of them are built taking groups of three C and the S consecutive atom). Each dihedral angle has a value of $\pm\pi$ in the *trans* configuration and 0 in the *cis* configuration. Thus, Θ_{S} may take values between 0 and 7 for octanedithiol, corresponding to all *cis* (hypothetical) and all *trans* configurations respectively.

Histograms of Θ_{S} and $d_{\mathrm{S–S}}$ were constructed from the results of the simulations, yielding the probability distributions shown in Fig. 2. This figure shows the frequency of occurrence of $d_{\mathrm{S–S}}$ and Θ_{S} for the four different types of junction configuration analyzed here. In the first case, it is found that the most twisted configurations correspond to the case of the T–K structure, while the most stretched structure is found in the case of the T–T structure. Consistent with this behavior, it is found that significant differences arise between the $d_{\mathrm{S–S}}$ distributions for the T–T and the T–K structures. These differences are not minor, resulting in $d_{\mathrm{S–S}}$ average values of 9.6 Å and 11.1 Å for T–T and T–K, respectively. In spite of the differences that arise in the molecular configurations, the outcome for the conductance results is remarkably similar for the four geometries considered, as shown in Fig. 3. Some differences can be found for the case of the T–K structure, presenting somewhat larger conductances, but the most probable conductance is barely distinguishable in the four geometries.

Another factor that is usually mentioned in the literature as responsible for obtaining different conductances is the coordination of the S atoms with the Au substrate. According to the results of ref. 24 more defective surfaces result in larger S–Au substrate coordinations and thus in larger conductances. Although this trend

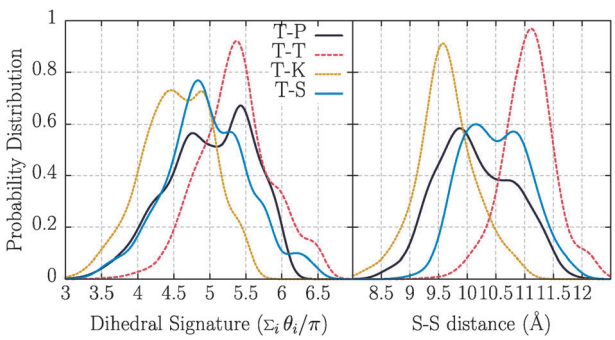

Fig. 2 Probability distributions of the dihedral signature Θ_{S} and sulfur–sulfur atom distances $d_{\mathrm{S–S}}$, as defined in the text, for the four metal junctions shown in Fig. 1.

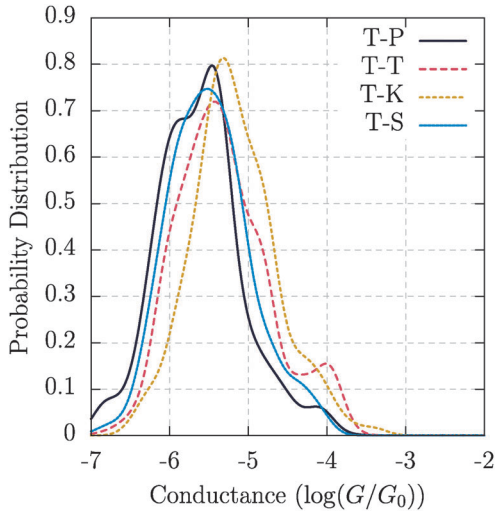

Fig. 3 Probability distribution of conductances for the four metal junctions shown in Fig. 1. It can be seen that the most probable conductance is very similar for the four geometries considered despite the differences in coordination of the S atom with the Au surface.

is qualitatively supported by the results of Fig. 3, since the conductance histograms are slightly shifted following the order ($G_{T-P} < G_{T-S} < G_{T-K}$), there is no indication for the occurrence of significantly different sets of conductances (say low, medium, high) as found in the experiments.

In our previous work we have shown that some particular molecular configurations, combined with the arrangement of the tip, may lead to increased conductance values of the system.[25] To analyze the effect of the molecule backbone–tip interaction on the conductance, we analyzed a fifth surface structure, consisting of a tip and a substrate with a small Au island. This structure results from cutting the first two lattice planes of a tip, attaching them to a perfect (111) surface and allowing for relaxation. This configuration is shown in Fig. 4, and can be expected to occur very often in STM break junctions, right after the rupture of the metal–metal bridge that is formed upon contact between the STM tip and the surface. The tip was positioned at 4 Å from the surface, and one of the ends of the molecule was set in contact with one of the upper planes of the tip, as shown in the figure. Different accelerated molecular dynamics runs were performed at different heights, obtained by lifting the tip. Fig. 5 contains cloud plots obtained at different retractions of the tip, reported in the legend of the figure. It is found that at short distances the carbon chain of the molecule somehow adheres to the tip. Upon tip retraction, the carbon chain detaches from the tip and finally stays nearly perpendicular to the surface. The corresponding conductance distributions are shown in Fig. 6. Dramatic changes are found in the conductance in the first retraction step, where the carbon chain is close to the tip surface (in the present case for distances ranging between 4.8 and 6.3 Å). The proximity between the chain and the tip allows direct tunnelling of the electron from the tip to the carbon chain leading to higher conductance. For distances larger than 6.3 Å, the conductances distribution remains roughly unaltered, and its most probable values stay close to those already discussed in Fig. 3. The occurrence of two well defined peaks at 4.8 and 6.3 Å is related to the anchoring of one of the S atoms to relatively stable

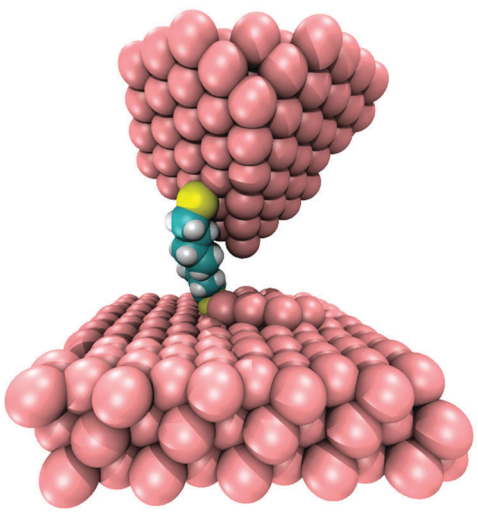

Fig. 4 Scheme of the tip–molecule–substrate configuration used to analyze the effect on the conductance of the site of attachment of the molecule to the tip. The figure shows the geometry of the closest approach between the tip and the surface. The other configurations, presented below in Fig. 5, were obtained by retraction of the tip.

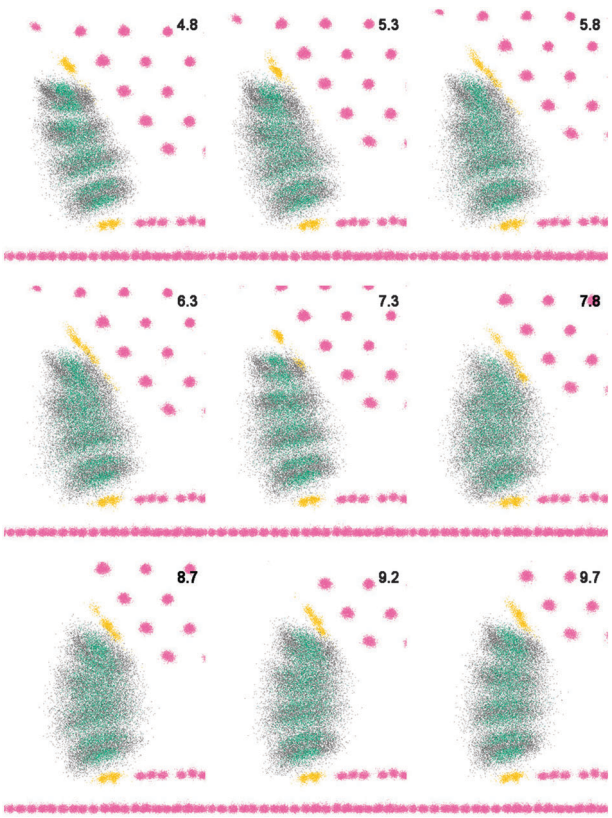

Fig. 5 Cloud plots obtained from the superposition of frames stemming from runs with the system depicted in Fig. 4. Green clouds correspond to the position of C atoms of the hydrocarbon chain, yellow ones to S atoms and pink ones to Au atoms. The tip–surface distances were in the increasing order of 4.8, 5.3, 5.8, 6.3, 7.3, 7.8, 8.7, 9.2 and 9.7 Å, respectively, as shown within each subfigure.

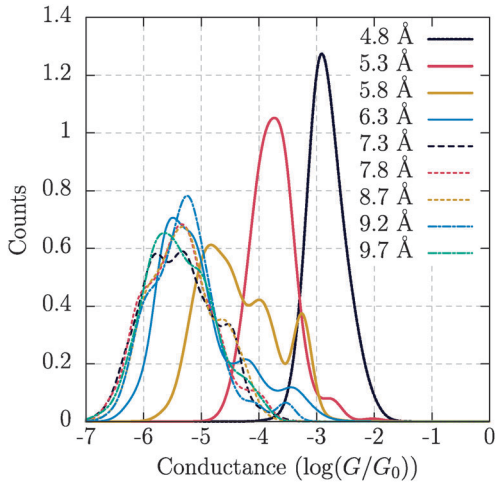

Fig. 6 Probability distribution of conductances corresponding to different tip–substrate distances for the system shown in Fig. 4 and 5. For short distances, where the carbon chain is close to the tip surface high average conductances are obtained. For distances larger than 6.3 Å, the conductances distribution remains around conductance averages close to those already shown in Fig. 3. The occurrence of two well defined peaks at 4.8 and 6.3 Å is related to the anchoring of one of the S atoms to relatively stable adsorption sites on the tip. This allows a close contact between the carbon chain and the tip which increases the conductance of the system.

adsorption sites on the tip, mainly defined by the sequence of lattice planes. This anchoring allows close contact between the carbon chain and the tip increasing conductance as described above.

Thus, the present results suggest that the occurrence of sets of conductances (low, medium, high) may be related to specific anchoring sites on the tip. While this could seem questionable on the basis of the argument that the orientation of the lattice planes on the tip should be at random on a statistical basis, this is not so. Molecular dynamics simulations have shown that when a tip is in contact with a surface, the former tends to "copy" the structure of the latter. For example, Table 1 of ref. 36 shows that when a (110) oriented tip interacts with a (111) surface, up to four layers of the tip may "copy" the structure of the substrate. This effect may be even stronger for a disordered tip.

A comment must be added when a quantitative comparison is attempted between present results and experiment. The present theoretical results should, in principle, be valid for experiments performed under vacuum, while experiments are usually performed in air or in the liquid phase. These different conditions represent very different situations for electron tunnelling. For instance, in ref. 24, the reported value of the slope $d\ln(I)/ds$ (I – tunnelling current, s – absolute tip sample separation) is (10 ± 1.5) nm^{-1}, resulting in an effective barrier of the order of 1 eV. However, experiments in UHV for an Au(111) surface yield barriers of the order of 3.6 eV.[37] Whatever the reason for the relatively low values obtained for the measurements in air or in the liquid phase, this will result in an increased penetration of the electrons in the gap. Thus, the effect of increased conductances will probably be observed in experiments at larger distances than those predicted from the present calculations.

4 Conclusions

In the present work we have used accelerated molecular dynamics simulations along with quantum conductance calculations to analyze the conductance of an alkanedithiol molecule confined in a metal–metal gap.

It is found that the (average) molecular configuration and the type of contact of the molecule with the surface plays a *minor role* in determining the conductance of the system.

On the other hand the anchoring sites of the molecule to the tip define the interaction of a portion of the molecule with it, playing the predominant role by keeping the carbon chain in close contact to the tip, thus increasing conductance.

Acknowledgements

We acknowledge financial support from CONICET PIP: 112-200801-000983, Secyt Universidad Nacional de Córdoba, Program BID (PICT-BICENTENARIO-2010-123), and PME: 2006-01581. S.A.P. and J.A. O.-A. thank CONICET for fellowships.

References

1 S. Guo, J. Hihath, I. Dez-Pérez and N. Tao, *J. Am. Chem. Soc.*, 2011, **133**, 19189–19197.
2 P. Makk, D. Tomaszewski, J. Martinek, Z. Balogh, S. Csonka, M. Wawrzyniak, M. Frei, L. Venkataraman and A. Halbritter, *ACS Nano*, 2012, **6**, 3411–3423.
3 R. J. Nichols, W. Haiss, S. J. Higgins, E. Leary, S. Martin and D. Bethell, *Phys. Chem. Chem. Phys.*, 2010, 1–29.
4 C. Li, I. Pobelov, T. Wandlowski, A. Bagrets, A. Arnold and F. Evers, *J. Am. Chem. Soc.*, 2008, **130**, 318–326.
5 B. Xu and N. J. Tao, *Science*, 2003, **301**, 1221–1223.
6 W. Haiss, R. J. Nichols, H. van Zalinge, S. J. Higgins, D. Bethell and D. J. Schiffrin, *Phys. Chem. Chem. Phys.*, 2004, **6**, 4330–4337.
7 F. Chen, J. Hihath, Z. Huang, X. Li and N. J. Tao, *Annu. Rev. Phys. Chem.*, 2007, **58**, 535–564.
8 X. Li, J. He, J. Hihath, B. Xu, S. M. Lindsay and N. Tao, *J. Am. Chem. Soc.*, 2006, **128**, 2135–2141.
9 T. Dadosh, Y. Gordin, R. Krahne, I. Khivrich, D. Mahalu, V. Frydman, J. Sperling, A. Yacoby and I. B. Joseph, *Nature*, 2005, **436**, 677.
10 C. Kergueris, J. Bourgoin, S. Palacin, D. Esteve, C. Urbina, M. Magoga and C. Joachim, *Phys. Rev. B: Condens. Matter Mater. Phys.*, 1999, **59**, 505–513.
11 A. A. Kornyshev and A. M. Kuznetsov, *Chem. Phys.*, 2006, **324**, 276–279.
12 A. A. Kornyshev, A. M. Kuznetsov and J. Ulstrup, *Proc. Natl. Acad. Sci. U. S. A.*, 2006, **103**, 6799–6804.
13 P. Vélez, S. Dassie and E. P. M. Leiva, *Phys. Rev. Lett.*, 2005, **95**, 2–5.
14 P. Vélez, S. Dassie and E. P. M. Leiva, *Chem. Phys. Lett.*, 2008, **460**, 261–265.
15 P. Vélez, S. Dassie and E. P. M. Leiva, *Phys. Rev. B: Condens. Matter Mater. Phys.*, 2010, **81**, 1–12.

16 M. E. Z. Michoff, P. Velez and E. P. Leiva, *J. Phys. Chem. C*, 2009, **113**, 3850–3854.
17 J. Olmos, M. Mariscal and E. Leiva, *Electrochim. Acta*, 2009, **54**, 2977–2982.
18 A. Aviram and M. Ratner, *Chem. Phys. Lett.*, 1974, **29**, 277–283.
19 K. Wang, N. L. Rangel, S. Kundu, J. C. Sotelo, R. M. Tovar, J. M. Seminario and H. Liang, *J. Am. Chem. Soc.*, 2009, **131**, 10447–10451.
20 C. F. A. Negre and C. G. Sánchez, *J. Chem. Phys.*, 2008, **129**, 034710.
21 S. Y. Quek, M. Kamenetska, M. L. Steigerwald, H. J. Choi, S. G. Louie, M. S. Hybertsen, J. B. Neaton and L. Venkataraman, *Nat. Nanotechnol.*, 2009, **4**, 230–234.
22 N. J. Tao, *Nat. Nanotechnol.*, 2006, **1**, 173–181.
23 *Recent advances in nanoscience*, ed. M. Mariscal and S. A. Dassie, Research Signpost, 2007.
24 W. Haiss, S. Martin, E. Leary, H. van Zalinge, S. J. Higgins, L. Bouffier and R. Nichols, *J. Phys. Chem. C*, 2009, **113**, 5823–5833.
25 S. A. Paz, M. E. Zoloff Michoff, C. F. A. Negre, J. A. Olmos-Asar, M. M. Mariscal, C. G. Sánchez and E. P. M. Leiva, *J. Chem. Theory Comput.*, 2012, **8**, 4539–4545.
26 A. F. Voter, *J. Chem. Phys.*, 1997, **106**, 111.
27 S. W. I. Siu, K. Pluhackova and R. a. Böckmann, *J. Chem. Theory Comput.*, 2012, **8**, 1459–1470.
28 D. Hamelberg, J. Mongan and J. A. McCammon, *J. Chem. Phys.*, 2004, **120**, 11919–11929.
29 K. E. Becker and K. A. Fichthorn, *J. Chem. Phys.*, 2006, **125**, 184706.
30 J. Olmos-Asar, A. Rapallo and M. Mariscal, *Phys. Chem. Chem. Phys.*, 2011, **13**, 6500–6506.
31 F. Chen, B. C. Curley, G. Rossi and R. L. Johnston, *J. Phys. Chem. C*, 2007, **111**, 9157–9165.
32 M. Allen and D. Tildesley, *Computer simulation of liquids*, 1989.
33 R. Landauer, *Philos. Mag.*, 1970, **21**, 873.
34 M. Büttiker, *Phys. Rev. Lett.*, 1986, **57**, 1761.
35 D. S. Fisher and P. A. Lee, *Phys. Rev. B: Condens. Matter Mater. Phys.*, 1981, **23**, 6851–6854.
36 M. Mariscal, C. F. Narambuena, E. P. M. Leiva and M. G. D. Pópolo, *Nanotechnology*, 2005, **16**, 974–980.
37 Y. Yamada, A. Sinsarp, M. Sasaki and S. Yamamoto, *Jpn. J. Appl. Phys.*, 2003, **42**, 4898–4900.
38 D. Q. Andrews, R. Cohen, R. P. Van Duyne and M. a. Ratner, *J. Chem. Phys.*, 2006, **125**, 174718.